Korean J. Chem. Eng., **23**(4), 531-539 (2006)

Prediction of concentration and temperature profiles for non-isothermal ethane cracking in a pipe reactor

Rajeev Kumar Garg, Venkatesan Venkat Krishnan and Vinod Kumar Srivastava†

Department of Chemical Engineering, Indian Institute of Technology, Hauz Khas, New Delhi-110016, India
(*Received 15 September 2005 • accepted 1 March 2006*)

Abstract−Thermal crackers are mostly modeled as plug flow systems, disregarding the lateral gradients present. In this paper, a 2-dimensional model has been established for ethane cracking in a thermal cracker in laminar flow, using a molecular mechanistic model for ethane cracking. The model, consisting of 9-coupled partial differential equations, is solved using the backward implicit numerical scheme. The resulting product distribution and temperature profiles are predicted throughout the reactor. The concentrations of acetylene and propylene show a maximum within the reactor. The effect of certain operational parameters - tube radius, wall temperature and mass flow rate - is also studied on these profiles. The parameters are varied in the range of 0.005-0.0125 m for tube radius, 1.25 kg/hr-2.5 kg/hr for mass flow rate and 850-1,050 °C for tube wall temperature. It is observed that an increase in wall temperature and an increase in tube radius or decrease in flow rate favours the conversion of ethane.

Key words: Thermal Cracker, Pipe Reactor, Coupled Partial Differential Equations, 2-Dimensional Modeling, Operational Parameters

INTRODUCTION

Ethylene is primarily produced by the thermal cracking of hydrocarbons. The thermal cracking reaction is carried out in long empty tubes embedded in a furnace. The empty tube, or the pipe reactor, is utilized in petrochemical plants and polymer synthesis sections for carrying out the reactions. Although with the advent of catalytic cracking, more and more catalytic crackers are being installed, thermal cracking is still used extensively because of its striking advantage in terms of its simplicity vis-à-vis the fact that it is not sensitive to the presence of various impurities in the feed. There is no requirement of pretreating the feed, to take care of sulphur, metals etc. which are poisons for the catalytic operations. Thermal cracking is widely practiced for vis-breaking and production of olefins [Filho and Sugaya, 2001; Holmen et al., 1995]. This technique has also shown promise for the disposal of polymers by their thermal destruction with the evolution of certain smaller valuable species [Bockhorn et al., 1998; Moringiu et al., 2003].

In thermal cracking, because of endothermicity of the process, the reaction material has to be supplied heat from outside, to maintain the pace of reactions; hence, the reactor essentially operates under non-isothermal conditions. There exist radial and axial concentration and temperature gradients, and hence reaction rates vary in both the directions. The various possible models developed for these reactors can be classified as one-dimensional model-assuming complete lateral mixing, or two-dimensional model-considering gradients both in axial and lateral directions. In a number of studies [Edwin and Balchen, 2001; Niaei et al., 2004; Pant and Kunzru, 1996; Ramana Rao et al., 1988], plug flow model is assumed. In these studies the model consists of a set of ODEs for heat transfer effects, mass conservation and hydrodynamics. Xu et al. [2002] have proposed a fast operating algorithm for thermal cracking furnaces, for optimization of the steam crackers, which again is based upon the assumption of plug flow conditions.

Sundaram and Froment [1979] have compared the one-dimensional model to a two-dimensional model for a pipe reactor with a single molecular reaction considering both the laminar and turbulent flow regimes. In both the flow conditions, it has been established [Sundaram and Froment, 1979] that typical radial concentration and temperature profiles exist. It has been shown that the one-dimensional model gives better predictions, if an averaged Nusselt number from a 2-dimensional model is incorporated into the 1-dimensional model. In another study by the same authors [Sundaram and Froment, 1980], these findings have been reported to hold for 2-dimensional modeling of ethane thermal cracker for turbulent conditions. In the latter study, the reported simulation results [Sundaram and Froment, 1980] pertain to a single set of operating conditions, where wall temperature is varied along the reactor length and at the exit; some of the species yields are compared to actual results. The product distribution within the reactor has not been reported. Only the concentration profiles of ethane in both the directions are depicted. Froment [1992] has compared the radial temperature profiles in ethane cracking coils for one-dimensional and two-dimensional models. In literature, most of reported studies are based on the one-dimensional models and the 2-dimensional model has not been widely used, although the lateral gradients are significant even in turbulent flow.

In this study, a molecular mechanistic scheme of reactions for ethane cracking has been adapted from Sundaram and Froment [1977]. Based on these reactions, 2-dimensional model equations for all the components and temperature have been developed. The concentrations of all the species are predicted in axial and radial directions. The resulting product distribution is also predicted throughout the reactor. The model is a rigorous simulation of reaction conditions in lab scale reactors, which typically have dimensions 0.5-1 cm

†To whom correspondence should be addressed.
E-mail: vkschemiitd@yahoo.com

diameter by 0.5-1 m long and the flow regime in these reactors is laminar flow. In addition, 1-D model for the reactor is also used to simulate the reactor under two conditions - the same heat flux as 2-D model or same wall temperature conditions as 2-D model. The various parameters for the thermal cracker like reactor pipe radius, wall temperature etc. have been varied and the effects of these changes on the reactor performance are studied.

MODEL DEVELOPMENT

Thermal cracking is carried out in pipe reactor, to which, because of endothermicity, heat is supplied through the reactor wall. There is maximum temperature at the wall of the reactor. This results in difference in the rates of reaction radially, at various axial positions. Thus concentration and temperature gradients get set up in both the directions. These effects are formulated in the form of partial differential equations. The proposed model for ethane cracking in pipe reactor is based upon the following assumptions:

- The reactor operates under steady state conditions as the reactor has continuous flow that stabilizes and gives steady state.
- The flow regime is laminar as it is similar to a lab scale reactor.
- The wall temperature is maintained high and constant because heat is required for the system from outside (endothermicity of system).
- No effect of temperature on physical properties and velocity profile.
- The axial diffusion and conduction are negligible in comparison to the convective flow of mass and heat respectively.
- The gradients in θ direction are not considered, as circumferentially uniform heating of the reactor is considered.

The reaction scheme to be used in this model is a molecular reaction scheme proposed by Sundaram and Froment [1977], for ethane cracking. This molecular model has been developed by using the radical reactions as a guide [Sundaram and Froment, 1977]. The main radical reactions responsible for ethane decomposition into ethylene are:

$$C_2H_6 + H^* \longrightarrow C_2H_5^* + H_2$$
$$C_2H_5^* \longrightarrow C_2H_4 + H^*$$

The sum of these two reactions yields the first equivalent molecular reaction of the scheme for ethane dehydrogenation. Similarly, the other reactions have been proposed in this model. The second molecular reaction for ethane decomposition is assumed to be first order and non-elementary whereas the other reactions are elementary [Sundaram and Froment, 1977]. The molecular reaction scheme is as follows:

$$C_2H_6 \underset{k_2}{\overset{k_1}{\rightleftharpoons}} C_2H_4 + H_2 \qquad \Delta H_1$$
$$2C_2H_6 \xrightarrow{k_3} C_3H_8 + CH_4 \qquad \Delta H_2$$
$$C_3H_6 \underset{k_5}{\overset{k_4}{\rightleftharpoons}} C_2H_2 + CH_4 \qquad \Delta H_3$$
$$C_2H_4 + C_2H_2 \xrightarrow{k_6} C_4H_6 \qquad \Delta H_4$$
$$C_2H_4 + C_2H_6 \xrightarrow{k_7} C_3H_6 + CH_4 \qquad \Delta H_5 \qquad (1)$$

These reactions involve a total of eight species (designated as A to H) in five reactions, two of them being reversible. The model should predict the concentrations of each of these species and the temperature of the reacting mass. The mass balances for each of the species and the overall heat balance have to be considered. The balances are written for a cylindrical shell of dimensions δz and δr at a distance z from the entrance and a distance r from the centre.

The mass balance for the i-th species takes the form:

$$\frac{D_{mi}}{r}\frac{\partial}{\partial r}\left[r\frac{\partial(C_i)}{\partial r}\right] - v_z\frac{\partial(C_i)}{\partial z} - (-r_i) = 0 \qquad \text{where i=species A, B....H} \quad (2)$$

In the above Eq. (2) axial diffusion of mass is neglected in comparison to convective transport in axial direction as

$$v_z\frac{\partial(C_i)}{\partial z} >> D_{mi}\frac{\partial^2(C_i)}{\partial z^2}$$

For each of the species a rate of dissociation can be written. For ethane (A) the rate of dissociation is given by

$$r_A = k_1C_A - k_2C_BC_H + k_3C_A + k_7C_BC_A \qquad (3)$$

On simplifying, the equations take the form

$$\frac{\partial^2(C_i)}{\partial r^2} + \frac{1}{r}\frac{\partial(C_i)}{\partial r} - \frac{v_z}{D_{mi}}\frac{\partial(C_i)}{\partial z} = \frac{1}{D_{mi}}(-r_i) \qquad (4)$$

The rate constant for ith reaction, is given by Arrhenius Law as

$$k_i = k_{i0}\exp\left[-\frac{E_i}{R(T+273)}\right] \qquad (5)$$

For endothermic reaction the energy balance is

$$\frac{k_{th}}{r}\frac{\partial}{\partial r}\left[r\frac{\partial T}{\partial r}\right] - \rho v_z C_p\frac{\partial T}{\partial z} - \sum_i \Delta H_{ri}(-r_i) = 0 \qquad (6)$$

assuming $\rho v_z C_p\frac{\partial T}{\partial z} >> k_{th}\frac{\partial^2 T}{\partial z^2}$

On simplification, it becomes

$$\left[\frac{\partial^2 T}{\partial^2 r} + \frac{1}{r}\frac{\partial T}{\partial r}\right] - \frac{\rho C_p v_z}{k_{th}}\frac{\partial T}{\partial z} - \frac{1}{k_{th}}\sum_i \Delta H_{ri}(-r_i) = 0 \qquad (7)$$

The velocity profile is

$$v_z = u_m\left[1 - \frac{r^2}{R^2}\right] \qquad (8)$$

The boundary conditions for this model are taken as: axial symmetry in the reactor; at the wall, temperature is constant and no diffusion of mass across the solid wall; at the entrance of the reactor, feed stream is at entrance conditions with no product species present in the feed stream.

$$r=0, \quad 0\le z\le L, \ \frac{\partial C_i}{\partial r} = 0, \ \frac{\partial T}{\partial r} = 0 \qquad (9a)$$

$$r=R, \quad 0<z\le L, \ \frac{\partial C_i}{\partial r} = 0, \ T=T_w \qquad (9b)$$

$$0\le r\le R, \ z=0, \ C_A=C_{A0}, \ C_B=C_C=\ldots=C_H=0, \ T=T_0 \qquad (9c)$$

This set of 8 mass balance equations (1 for each species), along with 1 equation for energy balance and the boundary conditions constitute the equations of the proposed model.

1. 1-D Model

The steady state model for plug flow conditions in the reactor (neglecting the lateral gradients) involves equations for a differential element of length δz and constant cross section area. The continuity equation for a component i can be given as

$$-v_a\frac{\partial(C_i)}{\partial z}=(-r_i) \tag{10}$$

The energy balance is

$$-\rho C_p v_a\frac{\partial T}{\partial z}-\sum_i \Delta H_{ri}(-r_i)=\frac{2}{R}q \tag{11}$$

The boundary conditions for this model at the inlet are

$$0\le r\le R,\ z=0,\ C_A=C_{A0},\ C_B=C_C=\ldots=C_H=0,\ T=T_0 \tag{12}$$

Using the same reaction scheme, the continuity equations are formulated for all the eight species. For the model solution, either a heat flux profile or wall temperature profile has to be incorporated. In this work, each of these profiles is imposed on 1-D model, the profile being exactly the same as that for 2-D model. The resulting set of ODEs has been solved by Runge Kutta fourth order method to simulate the profiles for 1-D model.

1-1. Data Availability

The required data to solve this model have been collected from various sources. The kinetic data for the reactions is as reported by Sundaram and Froment [1977]. The physical properties data has been taken from standard sources [Geankoplis, 1997; Perry, 1998; Yaws, 1999].

NUMERICAL SCHEME

The partial differential Eqs. (4) and (7) are second order in radial direction (r) and first order in axial direction (z). These sets of equations present the case of strong coupling among the nine PDEs (8 for mass balances and 1 for heat balance). Finite difference numerical method has been used to solve these nine coupled PDEs. The PDEs are discretized by utilizing the backward finite difference implicit scheme [Srivastava, 1983; Pareek et al., 2003].

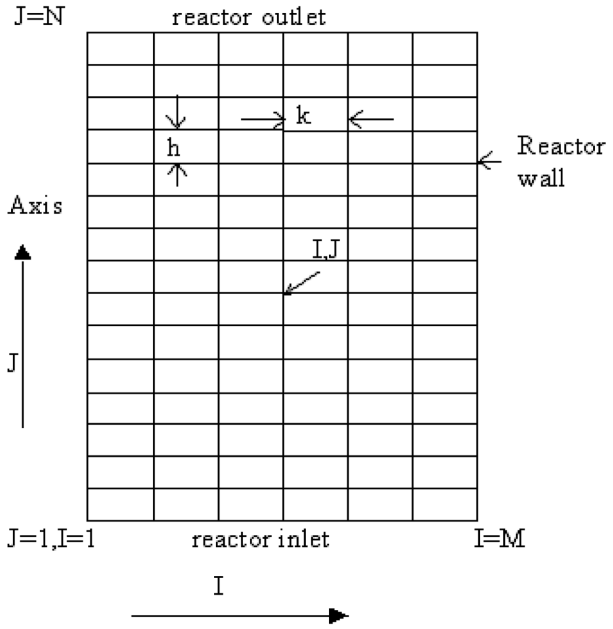

Fig. 1. Reactor grid system.

For discretization, the reactor domain chosen for analysis is divided into M-1 divisions in radial direction, k grid distance apart, and N-1 axial divisions, h grid distance apart. The radial step is designated as I(=1 to M) and axial step is J(=1 to N) as shown in Fig. 1.

The equivalent discretized equations, dropping the subscript for species, are

$$C_{J,I+1}\left[\frac{1}{k^2}+\frac{1}{2rk}\right]+C_{J,I}\left[-\frac{2}{k^2}-\frac{v_z}{D_m h}\right]+D_{J,I-1}\left[\frac{1}{k^2}-\frac{1}{2rk}\right]$$
$$=\frac{1}{D_m}\sum_l k_{l0}\exp\left[-\frac{E_l}{RT}\right]\prod_m\{(C_m)_{J-1,I}\}^{v_m}-\left[\frac{v_z}{D_m h}\right]C_{J-1,I} \tag{13}$$

The energy balance on discretization yields

$$T_{J,I+1}\left[\frac{1}{k^2}+\frac{1}{2rk}\right]+T_{J,I}\left[-\frac{2}{k^2}-\frac{v_z\rho_f C_p}{k_{th}h}\right]+T_{J,I-1}\left[\frac{1}{k^2}-\frac{1}{2rk}\right]$$
$$=\frac{1}{k_{th}}\sum_l \Delta H_{r,l}k_{l0}\exp\left[-\frac{E_l}{RT}\right]\prod_m\{(C_m)_{J-1,I}\}^{v_m}-\left[\frac{v_z\rho_f C_p}{k_{th}h}\right]T_{J-1,I} \tag{14}$$

The boundary conditions (Eqs. (9a), (9b), (9c)) convert to

$$I=1,\ J=1\ldots N\ \text{(axis of the reactor)},\ \frac{C_{J,I+1}-C_{J,I}}{k}=0,\ \frac{T_{J,I+1}-T_{J,I}}{k}=0$$
$$I=M,\ J=1\ldots N\ \text{(reactor wall)},\ \frac{C_{J,I}-C_{J,I-1}}{k}=0,\ T=T_W$$
$$I=1\ldots M,\ J=1\ \text{(reactor entrance)}$$
$$C_{A1,I}=C_{A0},\ C_{B1,I}=C_{C1,I}=\ldots=C_{H1,I}=0,\qquad T_{1,I}=T_0 \tag{15}$$

The Eqs. (13) and (15) involving concentrations are written for each of the 8 species. Each of these sets of equations for each species as well as the set for temperatures, written for a given axial position, can be represented in the matrix form **A.X**=**B**. The coefficient matrix **A** is a tridiagonal banded matrix of M*M dimension (M-1 * M-1 for temperature case). The coefficient matrix is transformed into a M*3 (M-1 * 3 for temp.) matrix through a transform technique developed by Srivastava [1983]. This transformation saves computing space and speeds up the computation process. The transformed system was solved by choosing an appropriate grid size and solving the system of difference equations at any given level I, J; using Srivastava's algorithm in FORTRAN. Through an iterative technique, the predicted results are improved upon at each step by iterating for the coupling term.

RESULTS AND DISCUSSION

The pipe reactor model is used to predict the reactor performance. The values of various variables and parameters for the reactor are given in Table 1. The physical properties have been estimated from standard data and correlations used in literature at an assumed value of temperature, higher than entrance temperature. At higher wall temperatures the average temperature of reaction mass is higher. It is found that the error in simulated results with assumption of no effect of temperature on physical properties and velocity profile and those incorporating temperature effects on physical properties and velocity profile are within 3-4%. The use of this simplifying assumption results in faster simulations. The various results generated are presented graphically. The radial and axial profiles for concentra-

Table 1. Values for variables and parameters

Variable/Parameter		Value							
Mass flow rate		0.15 kg/hr ethane+1.5 kg/hr nitrogen							
ρ		$3.5285*10^{-1}$ kg/m^3							
C_p		38.112 kJ/kg°C[b]							
k_{th}		0.06886 W/m°C[b]							
T_0		600 °C							
L		1.20 m							
ΔH_r		From standard sources as a function of temperature[b]							
k_{f0}		4.652×10^{13}, 3.85×10^{11}, 9.814×10^{8}, 1.026×10^{12}, 7.083×10^{13} s^{-1} or $l\cdot$mo$^{-1}\cdot$s^{-1}[a]							
E_i		272.5, 272.7,154.3,172.5, 252.6 kJ/mol[a]							
D	Species	A	B	C	D	E	F	G	H
	D*10^{-4} m^2/s[b]	1.17	1.23	0.93	0.96	1.31	.83	1.74	6.03

[a]Sundaram and Froment [1977].
[b]Geankoplis [1997], Perry [1998], Yaws [1999].

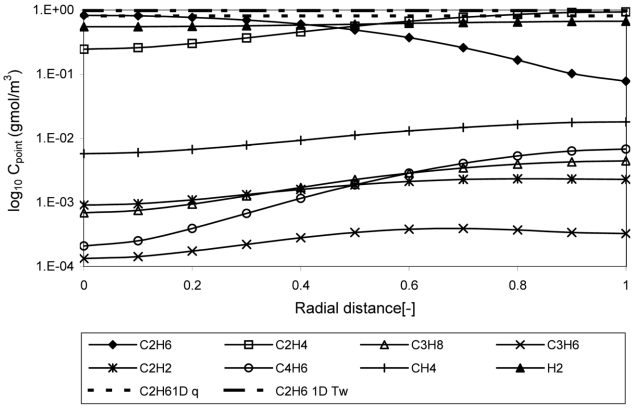

Fig. 2. Radial concentration profiles (R=0.01 m, T_w=950 °C, z=0.60 m, V=1.25 kg/hr).

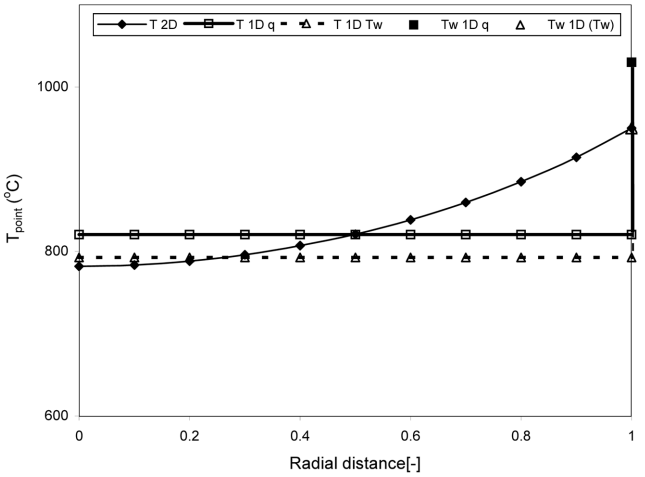

Fig. 3. Radial temperature profile (R=0.01 m, T_w=950 °C, z=0.60 m, V=1.25 kg/hr).

tions and temperature are shown in Figs. 2-15 for the different conditions (mentioned in the caption of the figure). The following observations can be made:

1. a) The radial concentration profiles (Fig. 2) clearly show the effect of variation in the reaction rates at the wall zone compared to the central zone due to temperature difference between the various zones. At z=0.60 m, the reactant ethane (A) reduces towards the wall, from $8.32*10^{-1}$ gmol/m^3 at centre to $7.82*10^{-2}$ gmol/m^3 at wall; whereas the products increase towards the wall (for ethylene (B), the concentration changes from $2.47*10^{-1}$ to $9.43*10^{-1}$ gmol/m^3 in moving from the centre towards the wall). The concentration of hydrogen (H) does not show any significant radial variation due to its high diffusivity compared to the other species. The concentration profile of ethane for 1-D model is flat (plug flow conditions) for both the conditions - same heat flux or same wall temperature as in 2-D model. For one-dimensional model, for both conditions (same q and same wall temperature) the ethane concentration profiles lie above that for 2-D model, showing lower extent of reaction for ethane if lateral gradients are neglected.

b) The Fig. 3 shows a radial temperature profiles at z=0.60 m. The temperature varies from 782 °C (centre) to 950 °C (wall) again explainable on the lines of concentration profiles. The region near the wall is having higher temperature compared to that near the axis, which results in different reaction rates at various radial locations. The radial temperature profiles for the plug flow model show that if the same heat flux is assumed, wall temperature is higher whereas process temperature is lower compared to that for 2-D model. On the other hand, for same wall temperature case, wall temperature is same but the process temperature for 1-D case is lower than 2-D case. This shows that neglecting radial gradients leads to lower temperature prediction and lower extent of reaction at any axial position.

2. a) Fig. 4 shows the axial average concentration of the various species. It is found that conversion of ethane (A) increases along the reactor length (concentration changes from 1.07 gmol/m^3 to $1.28*10^{-1}$ gmol/m^3) as well as the concentrations of ethylene, hydrogen, propane, butadiene and methane increase progressively into the reactor. On the other hand, the concentrations of propylene (D) and acetylene (E) increase and attain a maximum value and then show a slight decrease along the length of the reactor due to their being involved in various reactions as reactants and products. The con-

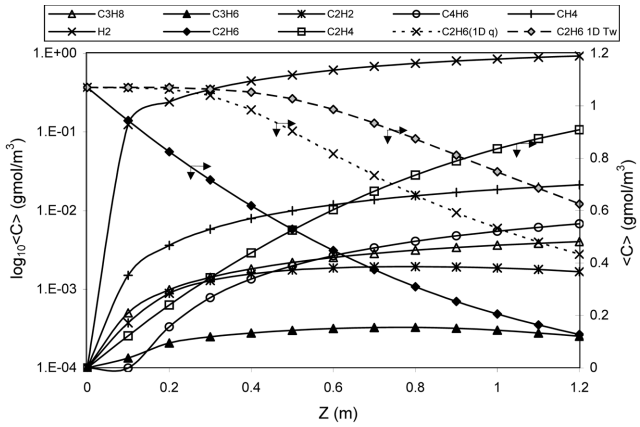

Fig. 4. Axial concentration profile (R=0.01 m, T_w=950 °C, V=1.25 kg/hr).

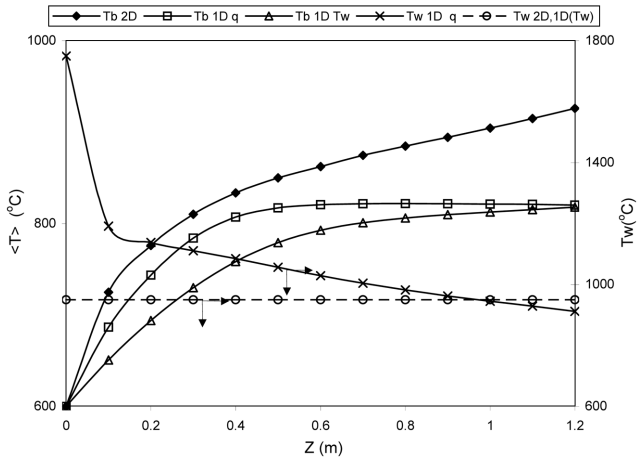

Fig. 5. Axial temperature profile (R=0.01 m, T_w=950 °C, V=1.25 kg/hr).

centration of butadiene (F) is not perceptible till around 0.10 m downstream of the reactor from its entrance. The ethane concentration profiles for 1-D model show that the conversion of ethane as predicted by neglecting radial profiles is lower as explained earlier.

b) The temperature gain along the reactor length is shown in Fig. 5. The reaction mass gets heated up from 600 °C at the entrance to an average value of 878.4 °C as it moves along despite consumption by reaction, due to conduction from the wall, whose temperature is being maintained constant. The bulk temperature and wall temperature profiles for 1-D model as compared to 2-D model are also depicted. For same heat flux, wall temperature is higher compared to 2-D case and the difference reduces along the length of reactor and towards the reactor exit, wall temperature for 1-D is

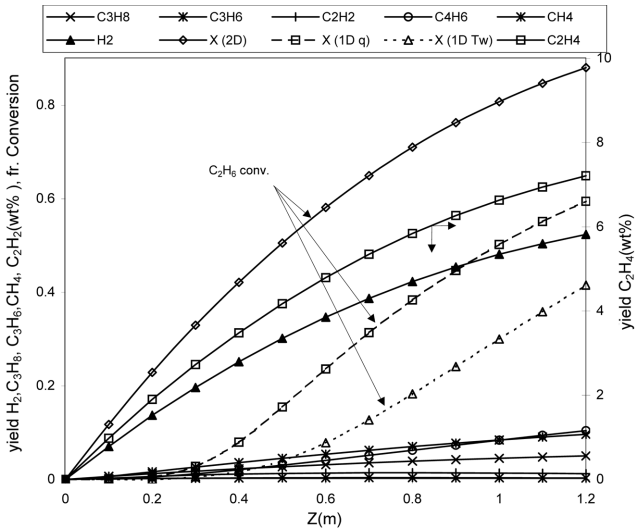

Fig. 6. Product yields vs ethane conversion (conditions as per Fig. 4 caption).

lower than that of 2-D due to reduced heat flux near the exit. The bulk temperature remains lower than that for 2-D case (820.3 °C 1-D same q, 817.9 °C 1-D same Tw, 878.8 °C for 2-D at exit). Similarly, if same wall temperature condition is imposed on the 1-D model, bulk temperature is lower than that for 2-D model. The lower bulk temperature in turn reduces the conversion.

3. Fig. 6 shows the yield of the various species as a function of conversion of ethane (A) for the conditions of Fig. 4. Ethane being the single feed component cracked, the conversion of ethane represents the severity of the cracking operation. It is observed that as the ethane conversion increases, the yields of the various product species increase. Ethylene (B) commands the maximum selectivity compared to all other product species at any conversion level. The yields of methane and hydrogen are the next highest among the products. The yields of acetylene and propylene show a maximum. The conversion profiles for ethane for the two cases of 1-D model are also depicted. It is found that 1-D model predicts lower conversion in both cases compared to 2-D case (59.46% 1-D same q, 41.56% 1-D same Tw and 88% for 2-D at exit).

Table 2 shows yields of various species and ethane conversion as given by the 2-D model and two cases of 1-D model. It is found that compared to 2-D model, 1-D models predict lower severity of cracking and hence lower yields of the products except that of propylene. Due to the same temperature and concentration of species in the cross section, ethylene and other product species cannot migrate to lower temperature zone. This leads to more conversion of ethylene to propylene. Thus, from these plots and table it is clear that

Table 2. Comparison of yields and conversion at reactor exit from 2-D and 1-D models (R=0.01 m, T_w=950 °C)

Yield (wt%)	C2H6	C2H4	C3H8	C3H6	C2H2	C4H6	CH4	H2	X
2D model	1.088	7.213	0.05	0.003	0.012	0.105	0.097	0.524	0.8804
1D (q)	3.687	4.961	0.032	0.005	0.014	0.007	0.035	0.356	0.5947
1D (Tw)	5.317	3.478	0.022	0.004	0.007	0.001	0.019	0.249	0.4155

neglecting radial gradients leads to under prediction of conversion, concentration and temperature in the reactor in general.

1. Effect of Parameters

In addition to the physical properties of the reaction mass, the operational or design parameters of the reactor have an influence on the extent of reaction and product distribution. The operational conditions of the reactor were varied, resulting in different reactor performance. The model is utilized to simulate the effect of operational aspects of the pipe reactor, which may influence the reactor yields. The chosen parameters are pipe radius, wall temperature and mass flux.

1-1. Effect of Pipe Radius

The radius of the reactor is varied in the range 0.005 m to 0.0125 m. Figs. 7, 8 and 9 show the effect of the variation of radius on the conversion of ethane, product yields (ethylene and methane) and temperature profiles, respectively, in the reactor. As the radius is decreased, at any axial position, the conversion of ethane (A) shows a decrease and the yields of product species decrease correspondingly (Figs. 7 and 8). At the reactor outlet, the concentration of A is $3.18*10^{-1}$ gmol/m^3 (R=0.005 m), $1.88*10^{-1}$ gmol/m^3 (R=0.0075 m), $1.28*10^{-1}$ gmol/m^3 (R=0.01 m) and $9.37*10^{-2}$ gmol/m^3 (R=0.0125 m). At R=0.005 m, there is no perceptible formation of methane till about 0.1 m downstream of the reactor entrance as shown in Fig. 8. This can be attributed to the increase in fluid velocity on decreasing the radius and hence a lower residence time. The temperature gain shows an increase as the radius is decreased (Fig. 9). The outlet temperature increases from 878.9 °C for R=0.0125 m to 883.2 °C for R=0.005 m, respectively. As the radius is decreased, the reaction decreases, taking up less heat. The conductive heat dominates over the convective loss and heat loss due to reaction, leading to higher temperature gain on decrease in the radius of the pipe.

1-2. Effect of Wall Temperature

The pipe reactor wall temperature is varied from 850-1,050 °C. The effect of wall temperature change is shown on the averaged quantities in Figs. 10, 11 and 12. The outlet concentration of ethane (A) is $5.49*10^{-1}$, $2.79*10^{-1}$, $1.28*10^{-1}$, $5.18*10^{-2}$, $1.57*10^{-2}$ gmol/m^3 for a wall temperature of 900, 950, 1,000, 1,050, 1,100 °C, respectively, and the corresponding conversions are shown (Fig. 10). It is clear from Fig. 10, that as per the predictions of the model, as the wall temperature is increased, the conversion of ethane (A) increases. This results in a corresponding increase in product species yields (Fig. 11). The reaction being endothermic, a higher temperature fa-

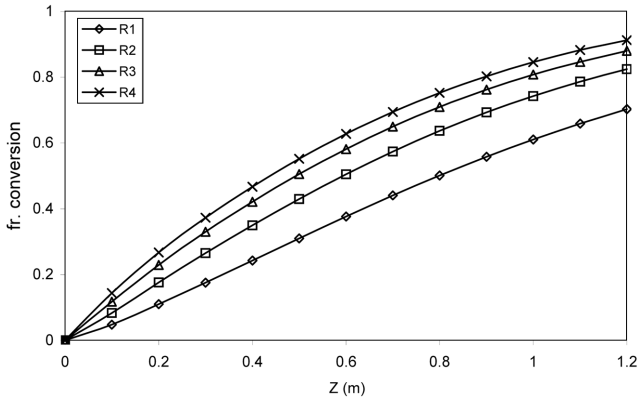

Fig. 7. Effect of pipe radius on ethane conversion (T_w=950 °C, R_1= 0.005 m, R_2=0.0075 m, R_3=0.01 m, R_4=0.0125 m, V=1.25 kg/hr).

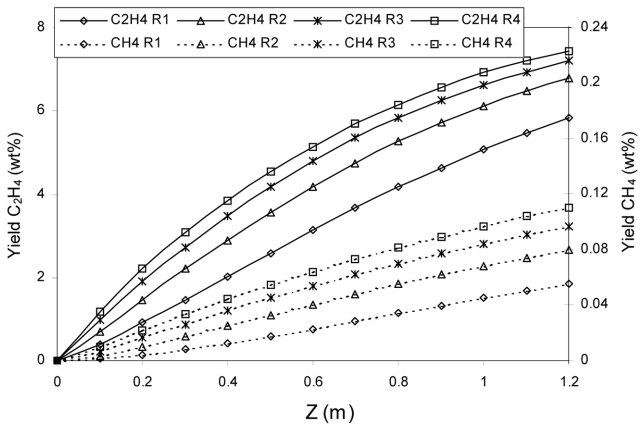

Fig. 8. Effect of pipe radius on product yields, C_2H_4 and CH_4 (T_w =950 °C, R_1=0.005 m, R_2=0.0075 m, R_3=0.01 m, R_4=0.0125 m, V=1.25 kg/hr).

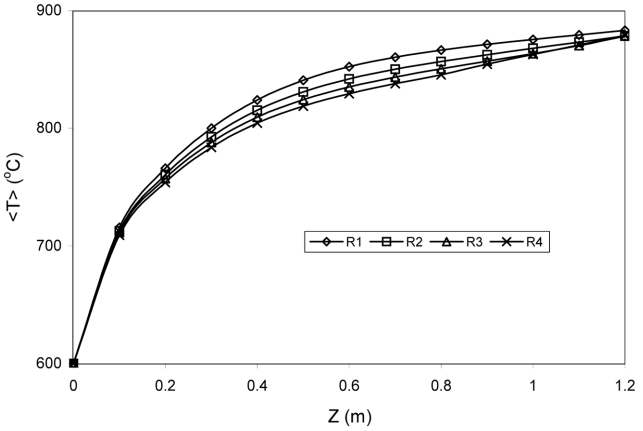

Fig. 9. Effect of pipe radius on axial temperature profiles (T_w= 950 °C, V=1.25 kg/hr, R_1=0.005 m, R_2=0.0075 m, R_3=0.01 m, R_4= 0.0125 m).

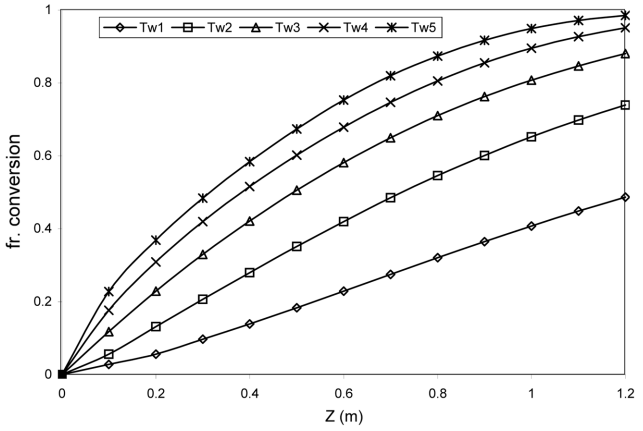

Fig. 10. Effect of wall temperature on ethane conversion (R=0.01 m, V=1.25 kg/hr, T_{w1}=850 °C, T_{w2}=900 °C, T_{w3}=950 °C, T_{w4}= 1,000 °C, T_{w5}=1,050 °C).

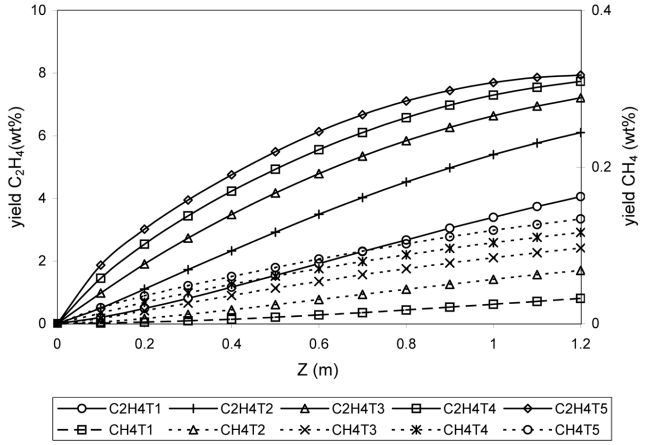

Fig. 11. Effect of wall temperature on product yields, C_2H_4 and CH_4 (R=0.01 m, V=1.25 kg/hr, T_{w1}=850 °C, T_{w2}=900 °C, T_{w3} =950 °C, T_{w4}=1,000 °C, T_{w5}=1,050 °C).

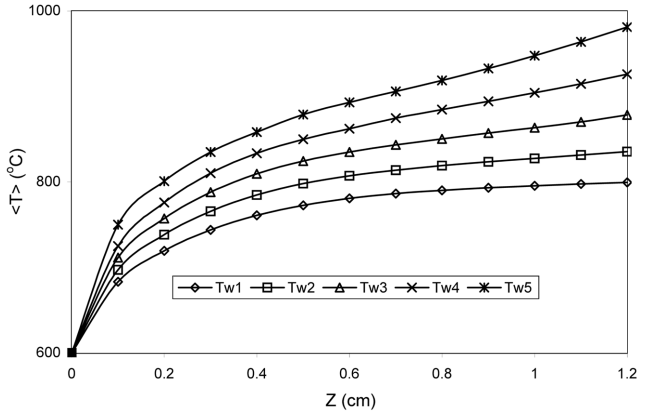

Fig. 12. Effect of wall temperature on axial temperature profiles (R=0.01 m, V=1.25 kg/hr).

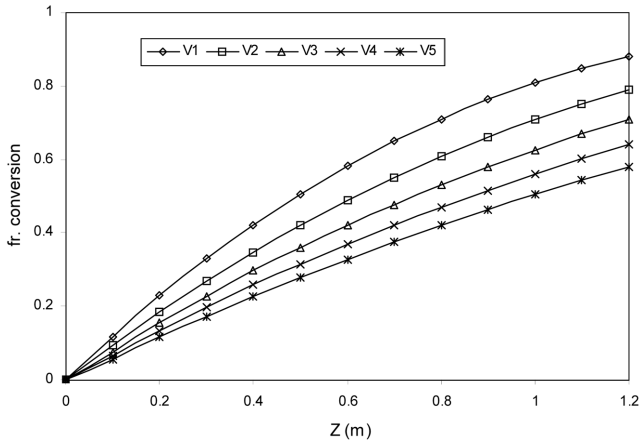

Fig. 13. Effect of mass flow rate on ethane conversion (R=0.01 m, T_w=950 °C, V_1=1.25, V_2=1.56, V_3=1.88, V_4=2.19, V_5=2.5 kg/hr).

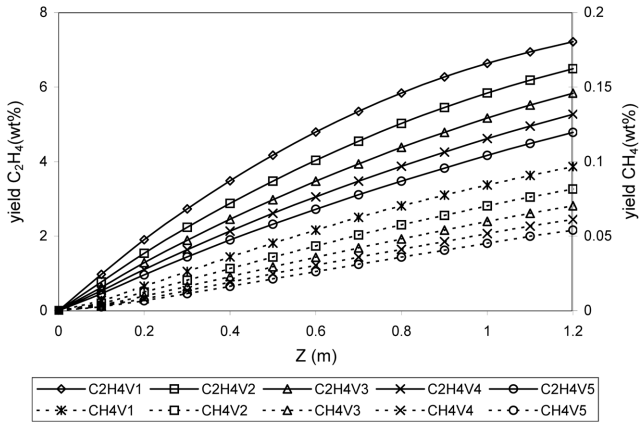

Fig. 14. Effect of mass flow rate on product yields, C_2H_4 and CH_4 (R=0.01 m, T_w=950 °C, V_1=1.25, V_2=1.56, V_3=1.88, V_4=2.19, V_5=2.5 kg/hr).

vours the reaction leading to higher concentration. of the product species. The predicted process average temperature (Fig. 12) also shows an increase as T_w is increased. This increase, despite more consumption by the reaction, can be explained on similar lines as discussed in pipe radius case.

1-3. Effect of Mass Flux

The effect of change in mass flow rate from 1.25 kg/hr to 2.5 kg/hr is shown in Figs. 13, 14 and 15. The effect of increase in mass flow rate amounts to an increase in velocity and hence a lower residence time. As the mass flow rate is increased, at any given location, the average conc. of ethane (A) increases, thereby lowering the conversion at that location (Fig. 13), whereas the concentrations of products decrease signaling lower yields of products due to lesser amount of reaction (Fig. 14, Table 3). The average temperature reduces on increase in mass flow rate (Fig. 15), although the effect is not so prominent. The two effects are explained as in the case of variation of tube radius.

CONCLUSIONS

Table 3. Average concentrations and temperature at z=0.60 m, R=0.01 m, T_w=950 °C

Mass flow rate (kg/hr)	Average concentration (gmol/m^3)								Avg. temp. (°C)
	A	B	C	D	E	F	G	H	
1.25	4.48E-1	6.04E-1	2.54E-3	3.17E-4	1.87E-3	2.68E-3	1.19E-2	6.12E-1	835.1
1.56	5.48E-1	5.08E-1	2.12E-3	2.96E-4	1.72E-3	1.85E-3	9.57E-3	5.14E-2	821.7
1.88	6.21E-1	4.38E-1	1.82E-3	2.78E-4	1.57E-3	1.34E-3	7.90E-3	4.42E-1	809.1
2.19	6.76E-1	3.85E-1	1.59E-3	2.63E-4	1.42E-3	1.00E-3	6.70E-3	3.88E-1	797.7
2.50	7.19E-1	3.43E-1	1.42E-3	2.50E-4	1.28E-3	7.73E-4	5.78E-3	3.46E-1	787.5

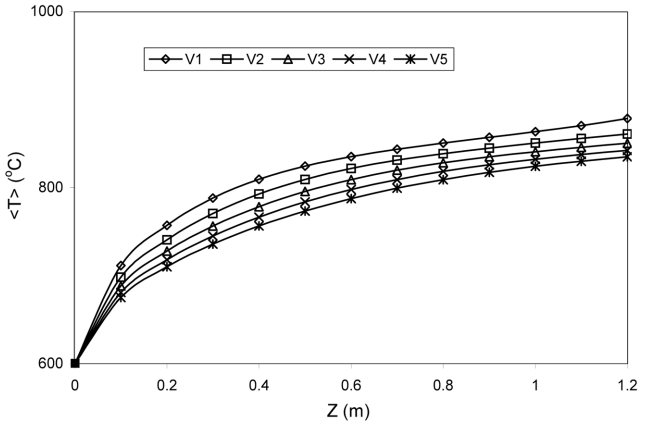

Fig. 15. Effect of mass flow rate on axial temperature profiles (R= 0.01 m, T_w=950 °C, V_1=1.25, V_2=1.56, V_3=1.88, V_4=2.19, V_5=2.5 kg/hr).

The simulation of the non-adiabatic non-isothermal pipe reactor for the ethane pyrolysis has been attempted using a 2-dimensional model. The simulated product distribution and temperature profiles are as expected. It is deduced that the typical radial variations in concentrations and temperature are there, demonstrating the dispersion and conductive effects. Due to the high diffusivity of hydrogen, the radial variation in its concentration is much less. The results obtained for the 2-dimensional model, when compared to those from the 1-dimensional model, show that if radial gradients are not considered lower conversion and temperature are predicted than that from 2-D model under similar heat flux or wall temperature conditions. It is also observed that either increasing the pipe radius and wall temperature or decreasing the flow velocity of the reacting material can give an increase in ethane conversion.

NOMENCLATURE

A : ethane
B : ethylene
C : propane
$C_{I,J}$: conc of species i (discretized form) [gmol/m^3]
C_i : conc of species i [gmol/m^3]
C_{i0} : conc of species i at entrance of reactor [gmol/m^3]
C_{AVG} : average concentration [gmol/m^3]
C_p : specific heat [kJ/kg°C]
D : propylene
$D_{m,i}$: diffusivity of species i [m^2/s]
E : acetylene
E_i : activation energy [kcal/mol]
F : butadiene
G : methane
H : hydrogen
h : step length in axial direction
$\Delta H_{r,i}$: heat of reaction i [kJ/gmol]
k : step length in radial direction
k_{th} : thermal conductivity [W/m °C]
k_i : reaction rate constant of reaction i [conc $^{1-n}$/s]
k_{i0} : frequency factor [conc $^{1-n}$/s]
L : length of reactor [m]
r : radius (local), radial coordinate [m]
R : pipe radius [m]
q : heat flux [J/m^2]
T : process temperature [°C]
<T> : average process temperature [°C]
T_0 : inlet temperature [°C]
T_w : wall temperature [°C]
u_m : max. velocity [m/s]
v_m : stoichiometric coefficient of species 'm' in reaction 'i'
v_z : local velocity [m/s]
v_a : average velocity [m/s]
V : mass flow rate [kg/hr]
X : conversion
z : reactor axial dimension [m]

Greek Letter

ρ : density [kg/m^3]

REFERENCES

Bockhorn, H., Hornung, A., Hornung, U., Jakobström, P. and Kraus, M., "Dehydrochlorination of plastic mixtures," *J. of Anal. Appl. Pyrolysis*, **49**, 97 (1999).

Edwin, E. H. and Balchen, J. G, "Dynamic optimization and production planning of thermal cracking operation," *Chem. Engg. Sci.*, **56**, 989 (2001).

Filho, R. M. and Sugaya, M. F., "A computer aided model for heavy oil thermal cracking process simulation," *Comput. and Chem. Engg.*, **25**, 683 (2001).

Froment, G. F., "Kinetics and reactor design in the thermal cracking for olefins production," *Chem. Engg. Sci.*, **47**, 2163 (1992).

Geankoplis, C. J., *Transport processes and unit operations*, Prentice Hall of India, New Delhi, 3rd Ed. (1997).

Holmen, A., Olsvik, O. and Rakstad, O. A., "Pyrolysis of natural gas: chemistry and process concepts," *Fuel Proc. Tech.*, **42**, 249 (1995).

Moringiu, A., Faravelli, T., Bozzano, G, Dente, M. and Ranzi, E., "Thermal degradation of PVC," *J. of Anal. Appl. Pyrolysis*, **70**, 519 (2003).

Niaei, A., Towfighi, J., Sadrameli, S. M. and Karimzadeh, R., "The combined simulation of heat transfer and pyrolysis reactions in industrial cracking furnaces," *Appl. Therm. Engg.*, **24**, 2251 (2004).

Pant, K. K. and Kunzru, D., "Pyrolysis of n-heptane: kinetics and modeling," *J. of Anal. Appl. Pyrolysis*, **36**, 103 (1996).

Pareek, V., Srivastava, V. K. and Adesina, A. A., "Modeling of absorption of NO_2 with chemical reaction in a falling raindrop," *Korean J. Chem. Engg.*, **20**, 328 (2003).

Perry, R. H. and Green, D. W., *Perry's chemical Engineers' handbook*, 7th Ed., Mc Graw Hill (1998).

Ramana Rao, M. V., Pliehers, P. M. and Froment, G. F., "The coupled simulation of heat transfer and reaction in a pyrolysis furnace," *Chem. Engg. Sci.*, **43**, 1223 (1988).

Srivastava, V. K., *The thermal cracking of benzene in a pipe reactor*, Ph.D. Thesis, University of Wales, Swansea, U.K. (1983).

Sundaram, K. M. and Froment, G. F., "A comparison of simulation models for empty tubular reactors," *Chem. Engg. Sci.*, **34**, 117 (1979).

Sundaram, K. M. and Froment, G. F., "Two dimensional model for the simulation of tubular reactors for thermal cracking," *Chem. Engg. Sci.*, **35**, 364 (1980).

Sundaram, K. M. and Froment, G. F., "Modeling of thermal cracking kinetics-1 thermal cracking of ethane, propane and their mixtures," *Chem. Engg. Sci.*, **32**, 601 (1977).
Xu, Q., Chen, B. and He, X., "A fast simulation algorithm for industrial cracking furnaces," *Hydrocarb. Proc.*, **81**, 65 (2002).
Yaws, C. L., *Chemical properties handbook: physical, thermodynamic, environmental*, McGraw Hill, NY (1999).